Journal of Visualization, Vol. 10, No. 1 (2007)75-82

Visualization of the Local Ionic Wind Profile in a DC Corona Discharge Field by Laser-Induced Phosphorescence Emission

Ohyama, R.*[1], Aoyagi, K.*[2], Kitahara, Y.*[2] and Ohkubo, Y.*[2]

*1 Department of Electrical Engineering, Tokai University, 1117 Kitakaname, Hiratsuka, Kanagawa, 259-1292, Japan. E-mail:rohyama@keyaki.cc.u-tokai.ac.jp
*2 Graduate School of Engineering, Tokai University, 1117 Kitakaname, Hiratsuka, Kanagawa, 259-1292, Japan.

Received 5 July 2006
Revised 19 September 2006

Abstract : Experimental visualization for ionic wind motion originated from DC corona discharges in a needle-plate electrode system has been investigated. A vapor-phase biacetyl tracer with laser-induced phosphorescence emission is used for optically characterizing the ionic wind profile. The ionic wind blows the excited biacetyl molecules away in continuing the visible phosphorescence emission for a long radiative lifetime. The captured image with elapsing time from the excitation presents the shifting location of radiative tracer along the ionic wind direction. The experimental results show the ionic wind profile enhanced in the electric field direction corresponding to the corona discharge progress. Especially, the ionic wind near an initiating point of corona discharges is focused as an advantage of this optical technique. The ionic wind velocity along the electrode axis can be obtained at the location close enough to the corona discharge initiation point, and the velocity at 0.5 mm from the discharge point is figured out as 9.3 to 19.2 m/s under the condition of the EHD Reynolds number of 0.95×10^3 to 2.1×10^3.

Keywords : Ionic wind, Phosphorescence emission, Flow velocity measurement, Corona discharge, Radiative tracer.

1. Introduction

Ionic wind is an electrohydrodynamically induced phenomenon in gases exposed to corona discharges. This phenomenon has been well known that the drifting single-polarity ions along the electric field direction can produce the neutral gas flow by a momentum transfer (Cobine, 1973), i.e., the ionic wind is considered as the local flow with drifting gas molecules. The ionic wind motion has been applied to enhancement of heat transfer effects (Franke and Hutson, 1982), improvement of electrostatic precipitators (Davidson, 1986; Mizeraczyk, 2003), and development of a gas-liquid two-phase electrohydrodynamic pump (Ohyama, 2005). The investigations on ionic wind characteristics have a number of experimental analyses including fluid flow measurements with manometer devices (Robinson 1961, Yabe, 1978, Chang, 1994, Labergue, 2005). The velocity analysis near a starting point of corona discharges is regarded as an important factor. However, the use of flow measurement devices for ionic wind fields is restricted away from the corona discharge region because the installed device is so large that it can no more be disregarded as compared to the discharge region. For the fluid flow analysis, it has been required without the influences of contact devices and charged tracer particles on the ionic wind sensitivity.

Gas-phase flow measurements based on laser-induced fluorescence imaging (Hanson, 2000; Deguchi, 2000) and laser-induced phosphorescence imaging (Hiller, 1984; Stier, 1999) with optical responsible molecules have been developed in gas jet flow analyses. The lifetime of fluorescence emission is the range of 10 ns as a standard. The effective lifetime of phosphorescence emission is much longer than the fluorescence emission. From several fundamental studies on phosphorescence lifetimes of laser-excited molecules, it has been known that biacetyl (2,3-butanedione) molecules have a long radiative lifetime of the order of 1.5 ms (Sidebottom, 1972). For the peak absorption wavelengths of 270 nm and 420 nm, the peak wavelength of phosphorescence emission is 525 nm in visible. In our previous work (Ohkubo, 2004), the influence of biacetyl molecules on the corona discharges has been evaluated from the analysis of measured conduction currents. From the results, it can be considered that there is no disturbance of vapor-phase biacetyl on the corona discharge characteristics. The use of phosphorescence emission from the excited biacetyl molecules will be an effective approach to the ionic wind analysis.

In this work, an experimental application of the laser-induced phosphorescence imaging to the visualization of ionic wind was investigated. The experiment was conducted in a DC corona discharge field formed with a simple needle-plate electrode arrangement, and filled with the vapor-phase biacetyl tracer. The visible phosphorescence emission of biacetyl molecules, which were excited by a pulsed laser beam of 266 nm in a wavelength, was appeared as a local profile of ionic wind motion with initiating corona discharges. Based on the experimental investigations, the local flow velocity was evaluated by an image analysis of the time-depended phosphorescence emission surrounding the corona discharge region.

2. Experimental Setup

The laser-induced phosphorescence imaging with biacetyl molecules has been used in this experiment. Figure 1 shows the schematic illustration of experimental setup to observe the local ionic wind motion in a corona discharge field. The electrode system was a needle-plate electrode

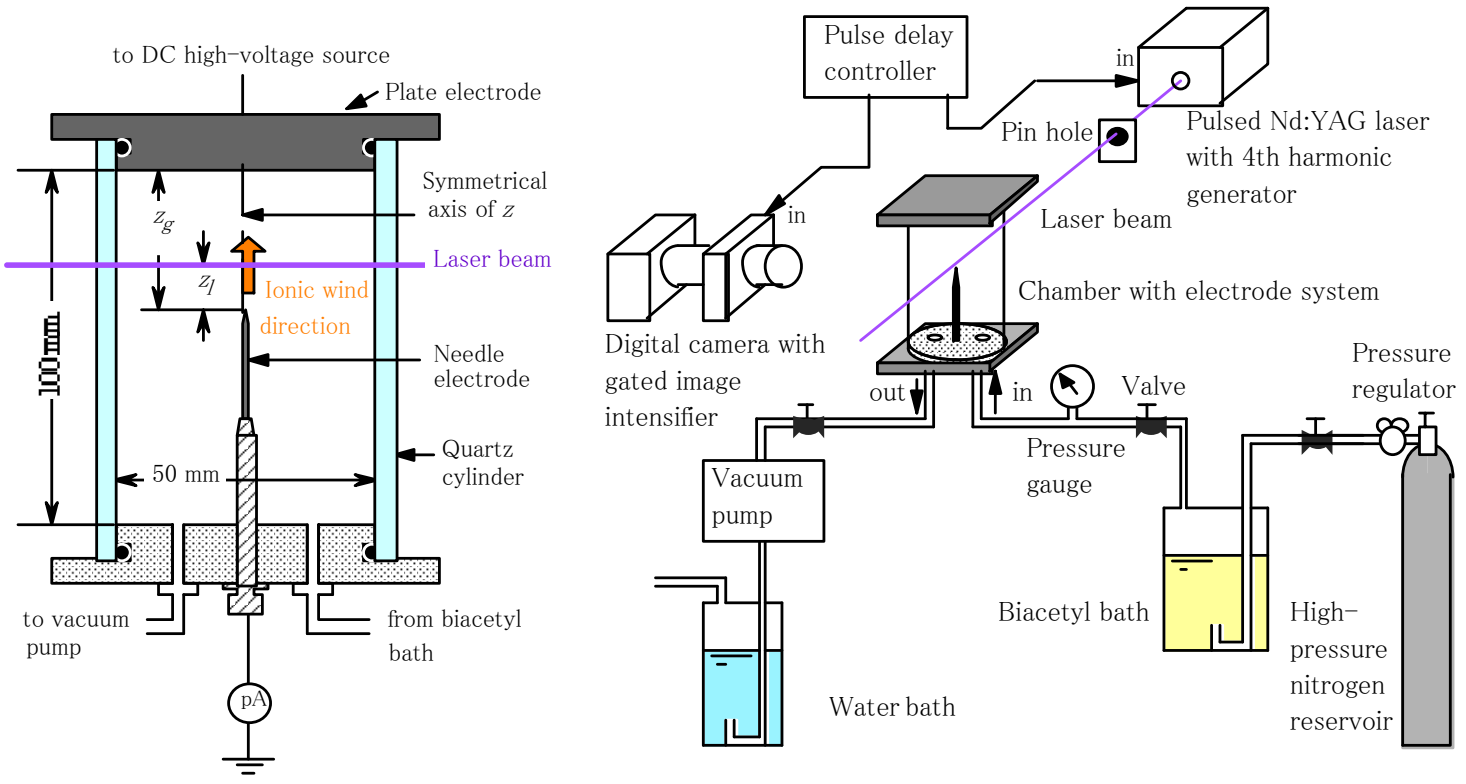

(a) Electrode system (b) Visualization system

Fig. 1. Schematic illustration of experimental setup.

arrangement vertically held in a cylindrical quartz glass chamber of an inner-diameter of 50 mm and a height of 100 mm as shown in Fig. 1(a). The top of chamber was the plate electrode made of aluminum, and connected to a DC high voltage source. The needle electrode made of steel with a diameter of 1 mm and a tip angle of 30 degrees was connected to the ground via a current measurement device (Keithley, 486 Picoammeter). In the symmetrical electrode system on the vertical axis of z, the location of needle electrode tip was defined as z = 0 and an electrode gap distance z_g was fixed to 15 mm.

As shown in Fig. 1(b), a visualization system consisted of a pulsed Nd:YAG laser (SolarLS, LG-129A-5-L) with a 4th-harmonic controller (SolarLS, LG-103-U) and a digital camera (Canon, EOS-D60) with a neighboring type gated image intensifier (Hamamatsu Photonics, V8070U-74-G130) connected to a pulse delay controller (BNC 555), a high-pressure nitrogen reservoir, a liquid biacetyl bath, and a vacuum pump. Vapor-phase biacetyl produced by bubbling the nitrogen gas through the biacetyl bath was filled into the chamber. The majority of oxygen molecules inside the chamber and the connecting gas tubes were evacuated by the vacuum pump to prevent quenching before the biacetyl tracer was enclosed. The density of liquid-phase biacetyl used was 980 kg/m^3, and the expected particle diameter for vapor-phase biacetyl introduced was the range of 0.1 to 10 μm orders in the fluorescence image and the phosphorescence image observed. The enclosed concentration of biacetyl was approximately 1059 ppm in the volume and the pressure of nitrogen/biacetyl mixing gas was adjusted to 0.1 MPa by a pressure regulator. The concentration of biacetyl was calculated by a following equation.

$$Biacetyl\ concentration = \frac{Consumption\ amount\ of\ biacetyl\,[\mathrm{mm}^3]}{Total\ volume\,[\mathrm{mm}^3]\times Number\ of\ repetitions}\times 10^6\,[ppm], \quad (1)$$

where *Number of repetitions* was 30, *Consumption amount of biacetyl* inside the biacetyl bath was 14922 mm^3 in the total of 30 repetitions, and *Total volume* of the chamber and the connecting gas tubes was 469732 mm^3. The influence of vapor-phase biacetyl tracer on the electrical discharge condition was considered from the conduction current as a function of the applied voltage V. The existence of biacetyl tracer slightly reduced the value of current, which the maximum reduced current was 1.0 μA in maximum applied voltage of 10 kV. This meant that the ionization of biacetyl particles was weak as compare with nitrogen gas.

The single beam from the pulsed laser, 266 nm in a wavelength and 10 ns in a pulse width, was passed through a pinhole of 0.5 mm in a diameter, and horizontally irradiated into the chamber. The biacetyl tracer was excited along the horizontal direction. The excitation position was focused on the symmetrical axis of z. The pulse delay controller for operating the pulsed laser shoot and the intensified image capture conducted the timing control in accuracy of sub-micro second order. An exposure time on the digital camera was fixed to 15 μs by gating the image intensifier. In the image capturing, the spatial and time resolving power was 73.6 pixels per mm and 10^5 s^{-1}, respectively.

In this experiment, the delayed time $\tau (= t_2 - t_1)$ from a laser shoot time t_1 to an image capture time t_2 was used as a variable factor for characterizing the phosphorescence emission. In addition, the focused initial location z_1 of laser beam for exciting the biacetyl molecules was used as another variable factor for considering the velocity distribution of ionic wind.

3. Experimental Results and Discussions

When the applied voltage V to electrode gap exceeded a corona discharge inception voltage of above 3.5 kV in this experimental condition, the initiation of ionic wind from the tip of needle electrode could be expected. The ionic wind was appeared as a local gas-phase movement simultaneously occurred with progressing the corona discharges along the needle electrode axis toward the plate electrode side. The time-averaged current measured for the applied voltages V of 6 kV to 10 kV, in case of the needle electrode in positive polarity, was the range of 2.7 μA to 15.9 μA with or without the vapor-phase biacetyl tracer. The EHD Reynolds number Re_{EHD} based on the discharge current has

been usually used as a fundamental parameter on ionic wind generations (Yamamoto, 1981; Ohkubo, 1990) and the ionic wind analyses have been examined in Re_{EHD} of the order of 10^3. The Re_{EHD} has been defined as a following equation.

$$\mathrm{Re}_{EHD} = \frac{U_{EHD} \cdot L}{\nu_g}, \text{ where } U_{EHD} = \sqrt{\frac{L \cdot i}{\rho_g \cdot \mu_i}}. \quad (2)$$

U_{EHD} m/s is the electrohydrodynamical characteristic velocity, L m is the characteristic length corresponding to an electrode gap distance, ν_g m^2/s is the kinematic viscosity of gas, i A/m^2 is maximum current density on the plate electrode, ρ_g kg/m^3 is density on gas, and μ_i m^2/Vs is the ion mobility of gas. In this experiment, the Re_{EHD} indicating the ionic wind generations from the needle electrode was the range of 0.95×10^3 to 2.1×10^3.

3.1 Visualization of Local Ionic Wind

Figure 2 shows the phosphorescence emission profiles near the needle electrode tip, when the applied voltage V was +10 kV and the initial excited location z_l was around 0.5 mm or 1.0 mm from the needle electrode tip. Here, the green area around the needle electrode tip was weak luminescence radiated from the corona discharges and different from the phosphorescence emission. This result indicated the shifting location of radiative tracer in the vertical direction for a period of τ because the ionic wind blew along the electrode axis corresponding to the major electric field direction. There was a remarkable displacement of the radiative tracer along the electrode axis and the phosphorescence emission profile was observed as a distorted line pattern. Although it seemed that the tracer particle size for phosphorescence emission images was enhanced to relative large scale with increasing the delayed time τ, the phosphorescence emission images with relative longer τ were presented due to the exhibition of sufficient distorted profiles. The location of phosphorescence emission was displaced gradually away from the initial location z_l with elapsing time τ as shown in Figs. 2 (b), (c) and (d). This result presented the shifting location of phosphorescence emission identified as a function of τ.

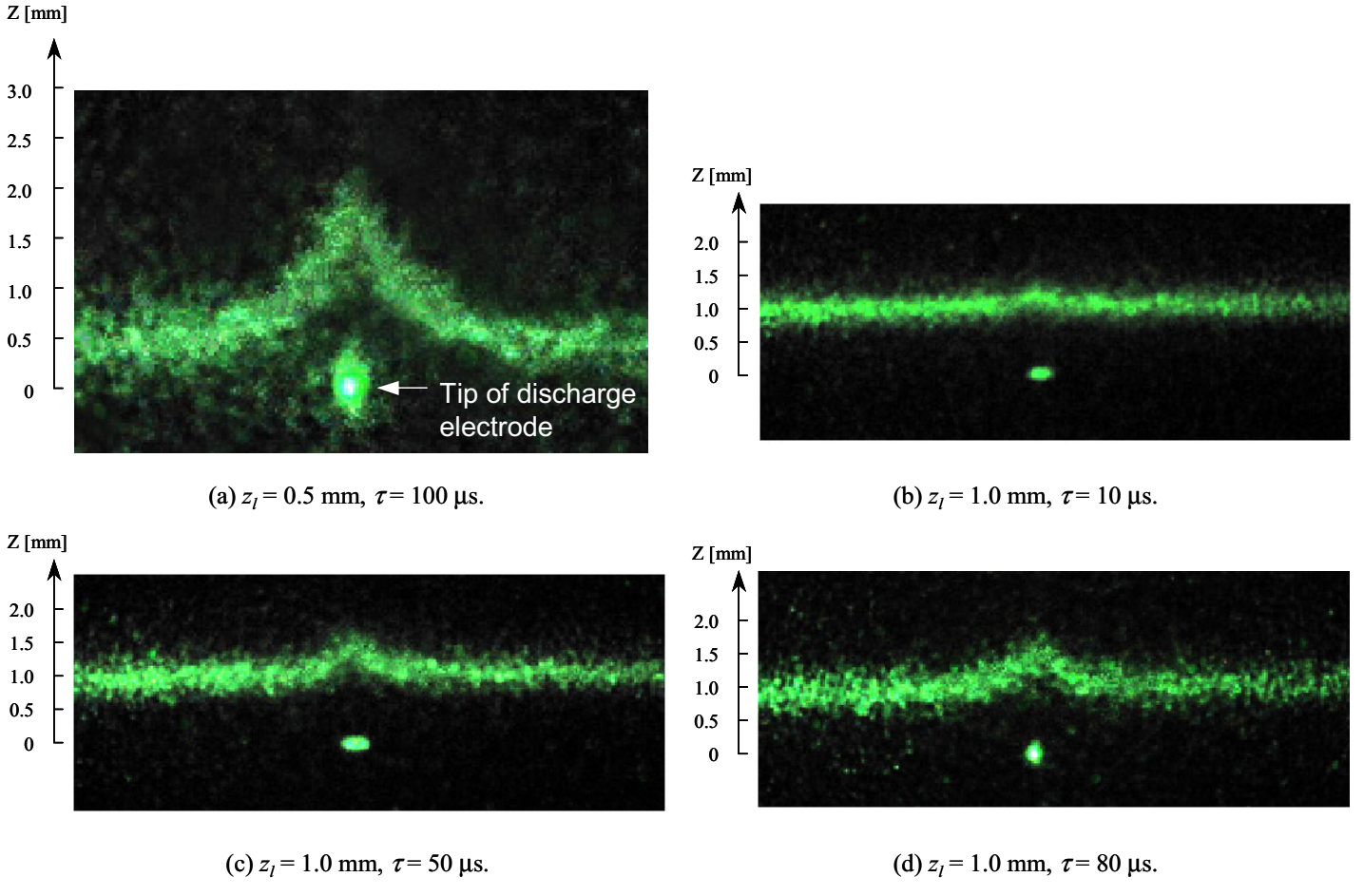

(a) z_l = 0.5 mm, τ = 100 μs.

(b) z_l = 1.0 mm, τ = 10 μs.

(c) z_l = 1.0 mm, τ = 50 μs.

(d) z_l = 1.0 mm, τ = 80 μs.

Fig. 2. Phosphorescence emission profiles. a, z_l = 0.5 mm and τ = 100 μs; b, z_l = 1.0 mm and τ = 10 μs; c, z_l = 1.0 mm and τ = 50 μs; d, z_l = 1.0 mm and τ = 80 μs.

Figure 3 shows a superposed picture of each phosphorescence emission image captured for varied initial locations z_1, when V was +10 kV and τ was expanded to 200 μs. Although the outlines of phosphorescence emission were not well formed due to the tracer diffusion with longer delayed time, it enabled us to recognize the distortion toward the plate electrode side. From these presented results, it could be visually understood that the convexo-shape pattern of phosphorescence emission profile was formed by the radiative tracer movements corresponding to the local ionic wind velocity on the symmetrical electrode axis in the vertical.

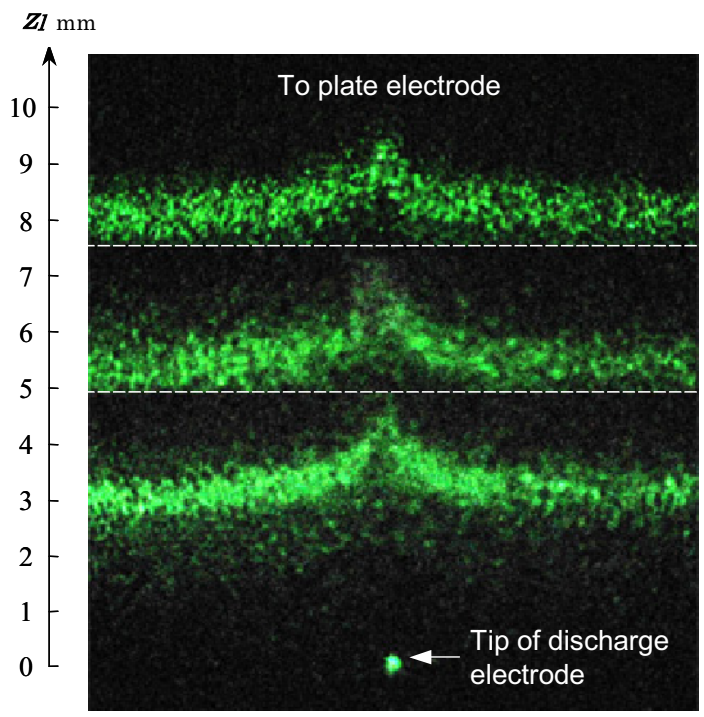

Fig. 3. Superposed picture of each phosphorescence emission image captured for varied initial locations z_1 of around 3.0, 5.5 and 8.0 mm, where V = +10 kV and τ = 200 μs.

3.2 Image Analysis for Local Ionic Wind Velocity

The experimentally obtained ionic wind profiles in the direction of corona discharge progress were emphasized along the symmetrical electrode axis of z. Since the phosphorescence emission images captured with a delayed time τ gave the displacement of radiative tracer in the ionic wind direction, the local velocity could be estimated by a simple image analysis as shown in Fig. 4. For sensitizing an arithmetic calculation in terms of the velocity and lessening diffusion of the radiative tracer, it was desirable to the delayed time τ as short as possible. From this reason, the analysis was conducted for the phosphorescence emission images under the delayed time τ to 50 μs. Figure 4(a) shows the explanatory example of a reference image with fluorescence emission (τ = 0 s) related to a time-delayed image with phosphorescence emission (τ = 50 μs), where the initial excited location z_1 was fixed to 1.0 mm. The enhancement gain of the image intensifier device was adjusted in higher for the phosphorescence image detection. The luminescence intensities were obtained from the fluorescence image and the phosphorescence image digitized to 8 bits by an image acquisition/processing system. Figure 4(b) shows each luminescence intensity of the reference image and the time-delayed image as a function of location z away from the needle electrode tip. Here, the vertical axis stands for an arbitrary unit and each plot means an averaged intensity among horizontal 11 pixels about each location on the z-axis, which is normalized with a maximum value of the fluorescence intensity. A peak location of fluorescence emission was corresponding to the initial excited location z_1 (= 1.0 mm), where the corona discharge luminescence at the needle electrode tip

(a) Explanatory example of reference image related to time-delayed image.

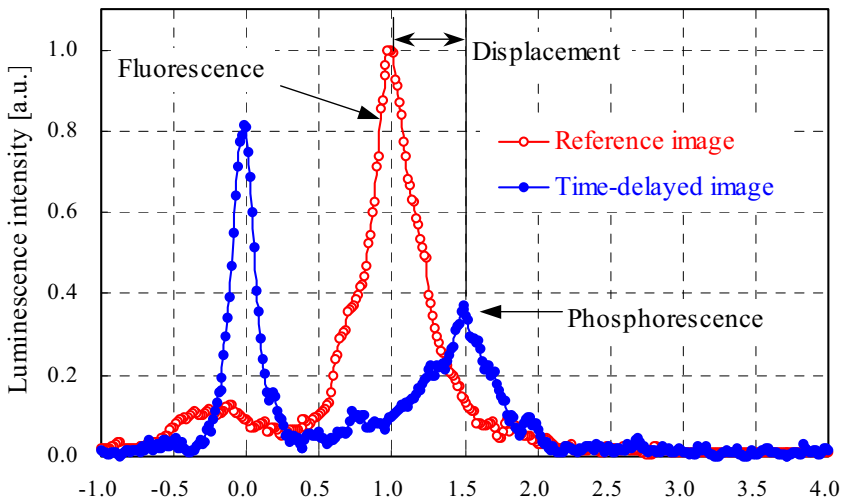

(b) Each luminescence intensity of reference image and time-delayed image as a function of location z from needle electrode tip.

Fig. 4. Luminescence distribution of reference image (τ = 0) and time-delayed image (τ = 50 μs) along symmetrical axis of z, where V = +10 kV and z_1 = 1 mm.

(z = 0) was eliminated in view of the explanation. The intensity of phosphorescence emission was weakened in comparison to the fluorescence emission and the peak location was appeared near 1.5 mm in the location z. The distance to the location (z = 1.5 mm) from the initial excited location (z = 1.0 mm) was considered to be a movement distance of radiative tracer for the period of τ(= 50 μs). The local ionic wind velocity u_z in the z-direction was estimated by using the distance and the delayed time τ.

Figure 5 shows the estimated velocity u_z of ionic wind as a function of the location z ($\geq$ 0.5 mm) from the needle electrode tip, where the average of 30 measurements for each initial excited location z_1 is plotted. It was confirmed that the velocity u_z was increased with increasing Re_{EHD}. As the advantage of this visualization technique, the ionic wind velocity u_z at the location close enough to the corona discharge initiation point could be experimentally obtained, and the velocity u_z at the location z of 0.5 mm was 9.3 to 19.2 m/s under the condition of the applied voltage V of 6 to 10 kV. Since the velocity u_z at the location z of 1.0 mm was 8.0 to 16.5 m/s, the velocity between the location z from 0.5 to 1.0 mm was reduced to 86 % due to the decreasing electric field intensity with increasing the distance z. It was expected that a peak in the velocity u_z was located in z < 0.5 mm because u_z was considered as 0 m/s at the boundary of z = 0 mm. Although this analysis was the local velocity identification at a focused single-spot, it enabled us to treat in much closer region to the starting point of corona discharges.

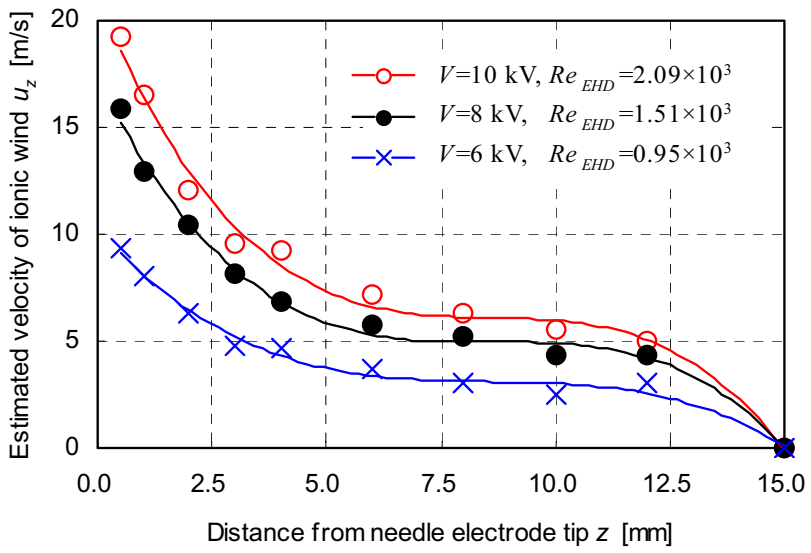

Fig. 5. Distribution of estimated ionic wind velocity u_z as a function of distance z from needle electrode tip for different EHD Reynolds number Re_{EHD}.

4. Conclusion

Ionic wind profiles near a DC corona discharge region originated at the tip of needle electrode were imaged by laser-induced phosphorescence emission from vapor-phase biacetyl tracer. In sustaining the phosphorescence emission with a relative long lifetime from the instantaneous laser-excitation, the vapor-phase biacetyl tracer was applicable to a radiative tracer blown away by the ionic wind.

This experiment was conducted for the ionic wind field with the Re_{EHD} of the order of 10^3. The experimental results presented the laser-induced phosphorescence emission profiles distorted from the initial excitation pattern with elapsing time. The profiles indicated the radiative tracer movements corresponding to the local ionic wind velocity in the major electric field direction.

The flow velocity at the location close enough to the discharge point was revealed through an analysis for the obtained phosphorescence emission images. The velocity distribution as a function of the location from the discharge point was presented. The velocity change between 0.5 mm and 1.0 mm from the discharge point was the range of 1.3 to 2.7 m/s under the condition of the applied voltage of 6 to 10 kV.

Acknowledgments

The authors are very grateful to the late Professor Kiyoji Kaneko for his guidance. This work is partly supported by grants from the Ministry of Education, Culture, Sports, Science and Technology of Japan, Research and Study Program of Tokai University Educational System general Research Organization.

References

Chang, J. S. and Watson, A., Electromagnetic Hydrodynamics, IEEE Trans. on Dielectrics and Electrical Insulation, 1-5 (1994), 871-895.

Cobine, J. D., Other Electrostatic Effects and Applications, Chapter 19, in: Moore, A.D. (Ed.), Electrostatics and Its Applications, (1973), A Wiley-Interscience Publication, New York.

Davidson, J. H. and Shaughnessy, E. J., Turbulence Generation by Electric Body Forces, Experiments in Fluids, 4 (1986), 17-26.

Deguchi, Y., Nakagawa, H., Ichinose, T. and Inada, M., LIF Applications for Practical Combustors, Journal of Visualization, 2-3/4 (2000), 343-353.

Franke, M. E. and Hutson, K.E., Effectc of corona discharge on the free-convection heat transfer inside a vertical hollow cylinder, ASME publication, 82-WA/HT-20 (1982).

Hanson, R., Baer, D., Morris, C., Thurber, M., Furlong, E. and Wehe, S., Recent Advances in Laser-based Diagnostics for Gaseous Flows, Journal of Visualization, 2-3/4 (2000), 309-321.

Hiller, B., Booman, R. A., Hassa, C. and Hanson, R. K., Velocity Visualization in Gas Flows using Laser-Induced Phosphorescence of Biacetyl, Rev. Sci. Instrum, 55-12 (1984), 1964-1967.
Labergue, A., Moreau, E. and Touchard, G., A Parametric Study of Surface Corona Discharge along an Insulating Flat Plate in Atmospheric Pressure, IEEE, 2005 Ann. Report Conference on Electrical Insulation and Dielectric Phenomena, (2005), 490-494.
Mizeraczyk, J., Dekowski, J., Podliński, J., Kocik, M., Ohkubo, T. and Kanazawa, S., Laser Flow Visualization and Velocity Fields by Particle Image Velocimetry in an Electrostatic Precipitator Model, Journal of Visualization, 6-2 (2003), 125-135.
Ohkubo, T., Hamasaki, S., Nomoto, Y., Chang, J. S. and Adachi, T., The Effect of Corona Wire Heating on the Downstream Ozone Concentration Profiles in an Air-Cleaning Wire-Duct Electrostatic Precipitator, IEEE Trans. on Industry Applications, 26-3 (1990), 542-549.
Ohkubo, Y. and Ohyama, R., Experimental Visualization of Corona Discharge Progress for Gas-Liquid Two-Phase EHD Flow Phenomenon, Proc. of 4th Int. Conference of the Electrostatic Society of France, (2004), 341-344.
Ohyama, R., Kumeta, M., Ueda, A., Watson, A. and Chang, J. S., A Fundamental Characteristic and Image Analysis of Liquid Flow in an AW Type EHD Pump, Journal of Visualization, 8-4 (2005), 339-346.
Robinson M., Movement of Air in the Electric Wind of the Corona Discharge, Trans. of AIEE, 80-1 (1961), 143-150.
Sidebottom, H. W., Badcock, C. C., Calvert, J. G., Rabe, B. R. and Damon, E. K., Lifetime Studies of the Biacetyl Excited Singlet and Triplet States in the Gas Phase at 25°, Journal of the American Chemical Society, 94 (1972), 13-19.
Stier, B. and Koochesfahani, M. M., Molecular Tagging Velocimetry (MTV) measurements in gas phase flows, Experiments in Fluids, 26 (1999), 297-304.
Yabe, A., Mori, Y. and Hijikata, K., EHD Study of the Corona Wind between Wire and Plate Electrodes, AIAA Journal, 16-4 (1978), 340-345.
Yamamoto, T. and Velkoff, H. R., Electrohydrodynamics in an Electrostatic Precipitator, J. Fluid Mech., 108 (1981), 1-18.

Author Profile

Ryu-ichiro Ohyama: He received his M.Sc.(Eng) in Electrical Engineering in 1988 from Tokai University. He also received his Ph.D. (Eng.) in Electrical Engineering in 1991 from Tokai University. He worked in Department of Engineering Physics, McMaster University as a visiting associate professor in 1999. He works in Electrical Engineering, Tokai University as an associate professor since 1996. His research interests are Quantitative Visualization in Electrohydrodynamically Induced Fluid Flow Field.

Kentaro Aoyagi: He received his B.Sc. (Eng.) in Electrical and Electronic Engineering in 2005 from Tokai University. He is currently studying at Graduate School of Engineering, Tokai University. His research interests are Quantitative Visualization in Electrohydrodynamically Induced Fluid Flow Field.

Yu Kitahara: : He received his B.Sc. (Eng.) in Electrical and Electronic Engineering in 2006 from Tokai University. He is currently studying at Graduate School of Engineering, Tokai University. His research interests are Quantitative Visualization in Electrohydrodynamically Induced Fluid Flow Field.

Yoko Ohkubo: She received her B.Sc. (Eng.) in Electrical Engineering in 2003 from Tokai University. She also received her M.Sc. (Eng.) in Electrical Engineering in 2005 from Tokai University. She currently works in Hitachi Co. Her research interests are Quantitative Visualization in Electrohydrodynamically Induced Fluid Flow Field.